

Solar abundances and helioseismology: fine structure spacings and separation ratios of low-degree p modes

Sarbani Basu

*Department of Astronomy, Yale University, P.O. Box 208101, New Haven, CT
06520-8101; sarbani.basu@yale.edu*

William J. Chaplin, Yvonne Elsworth

*School of Physics and Astronomy, University of Birmingham, Edgbaston, Birmingham B15
2TT, U.K.; w.j.chaplin@bham.ac.uk, y.p.elsworth@bham.ac.uk*

Roger New

*Faculty of Arts, Computing, Engineering and Sciences, Sheffield Hallam University,
Sheffield S1 1WB, U.K.; r.new@shu.ac.uk*

Aldo M. Serenelli

Institute for Advanced Study, Einstein Drive, Princeton, NJ 08540; aldos@ias.edu

and

Graham A. Verner

*School of Physics and Astronomy, University of Birmingham, Edgbaston, Birmingham B15
2TT, U.K.; gav@bison.ph.bham.ac.uk*

ABSTRACT

We have used 4752 days of data collected by the Birmingham Solar-Oscillations Network (BiSON) to determine very precise oscillation frequencies of acoustic low-degree modes that probe the solar core. We compare the fine (small frequency) spacings and frequency separation ratios formed from these data with those of different solar models. We find that models constructed with low metallicity are incompatible with the observations. The results provide strong support for lowering the theoretical uncertainties on the neutrino fluxes. These uncertainties had recently been raised due to the controversy over the solar abundances.

Subject headings: Sun: helioseismology - Sun: interior - Sun: abundances - neutrinos

1. Introduction

One of the key inputs used in constructing models of stars, including the Sun, is the heavy element abundance, Z , or the ratio of the abundance of heavy elements to that of hydrogen Z/X . Helioseismic studies of solar models constructed with the Grevesse & Sauval (1998; henceforth GS) abundance, and the even earlier Grevesse & Noels (1993) abundances, show a remarkable agreement with the Sun (e.g., Christensen-Dalsgaard et al. 1996; Bahcall et al. 1997; Morel et al. 1999; Basu, Pinsonneault & Bahcall 2000, etc.). The situation has changed in the recent years with the claim by Asplund et al (2001), Allende Prieto, Lambert & Asplund (2001, 2002), Asplund (2004), Asplund et al. (2004), Asplund et al. (2005), that the oxygen, carbon and nitrogen abundance in the Sun needs to be reduced. The reduction in the oxygen abundance implies the reduction of the abundances of other elements such as Ne, Ar also. This reduces the solar heavy element abundance from the GS value of $Z/X = 0.0229$ to $Z/X = 0.0176$. Asplund, Grevesse & Sauval (2005; henceforth AGS) presented a new table of abundances based on the above reduction. In addition, based on Asplund (2000) they reduced the silicon abundance (and thus lowered the abundance of all the meteoritic elements), and this reduced Z/X further to 0.0166. Solar models constructed with the new, low abundances do not satisfy the helioseismic constraints of the position of the convection-zone base and the helium abundance in the convection zone. Models with the lower heavy-element abundances are found to have too shallow a convection zone (henceforth CZ), and a helium abundance, Y , that is too low. Furthermore, the sound-speed and density profiles of the models do not match those of the Sun either (Bahcall & Pinsonneault 2004; Basu & Antia 2004; Bahcall et al. 2005a, 2005b, 2005c, 2006; Delahaye & Pinsonneault 2006). By looking at the structures of the main heavy-element ionization zones in the solar convection zone Antia & Basu (2006) argue that the solar heavy element abundance has to be high, i.e., close to the old GS values. Pinsonneault & Delahaye (2006) by considering the physics of stellar atmospheres also conclude that high CNO abundances are favored.

Almost all the helioseismic tests of solar models constructed with the new abundances have focused on the solar convection zone. Few studies have looked at what happens to the solar core. Where the core has been considered it has been through results of inversions, where inversion data on the core have been combined with results pertaining to the other parts of the Sun to give RMS deviations of the sound-speed and density profiles of the models with respect to those of the Sun (e.g., Bahcall et al. 2005a, 2006). In this work, we concentrate on the solar core. The solar core is, of course, where all the nuclear reactions take place, and where all the energy and neutrinos are released – hence the interest in what happens to the core when solar metallicity is reduced.

Only modes of low degree ($l = 0-3$) can be used to determine the structure of the solar

core. In this paper we report a study in which observed low-degree frequencies have been compared with those of several standard solar models constructed with different abundances. The solar p -mode data come from observations made by the ground-based Birmingham Solar-Oscillations Network (BiSON; Chaplin et al. 1996). The BiSON instruments make disc-averaged observations of the Sun in Doppler velocity. These observations have provided the field of helioseismology with high-quality, long-term monitoring of the low- l modes. Here, we use frequencies determined to excellent precision from a BiSON timeseries lasting 13 years.

The aim of this paper is to compare and contrast the frequencies of different solar models with those of the Sun in order to determine whether we can distinguish between models made with the older, higher abundances on the one hand and those made with the newer (AGS) abundances on the other. Our aim is then to see if we can rule out one set of abundances, thereby reducing the uncertainty in the solar abundances. This is particularly relevant for the study of solar neutrinos. Recently the theoretical uncertainty on solar neutrinos had been raised because of the uncertainty in the solar abundances (Bahcall & Serenelli 2005, Bahcall et al. 2006). The uncertainties in the values of the heavy-element abundances of the Sun are the largest source of the theoretical uncertainty in calculating the p - p , pep , 8B , ${}^{13}N$, ${}^{15}O$, and ${}^{17}F$ solar neutrino fluxes (Bahcall & Serenelli 2005). The difference between the GS and AGS abundances is larger than the error-bars on each of the abundances, and hence Bahcall & Serenelli (2005) and Bahcall et al. (2006) calculated the uncertainties in the neutrino fluxes by designating the difference between GS and AGS values as the uncertainty in the composition. In this work we try to examine if data on the low-degree modes are of sufficient quality to distinguish between models with the older, higher abundances and those with the newer, lower abundances and hence to thereby reduce the neutrino uncertainties to pre-AGS levels.

A simple comparison of the frequencies of the Sun and solar models is often not very informative. One reason is that all the modes sample the outer layers of the Sun, and hence even low-degree modes do not have localized information on the solar core. Another reason is that the physics used in the solar models does not reproduce the structure of the near-surface layers very well: the main culprit is the very basic treatment of convection, generally using the mixing length theory, which breaks down close to the surface, another factor is that the assumption of adiabaticity, used in the calculation of the frequencies of solar models, breaks down near the solar surface. Both these errors, and other uncertainties relating to the solar surface, give rise to frequency errors that are functions of frequency alone (e.g., Cox & Kidman 1984; Balmforth 1992 and discussion in Christensen-Dalsgaard 2002). To study the core one therefore, normally compares the so-called *fine* or *small frequency spacings* of the low- l p modes given by the combination.

$$d_{ll+2}(n) = \nu_{n,l} - \nu_{n-1,l+2}, \quad (1)$$

where ν is the frequency of a mode of degree l and radial order n . The frequencies $\nu_{n,l}$ and $\nu_{n-1,l+2}$ are very similar and hence are affected in a similar way by near-surface effects. By taking this difference in frequency a large part of the effects from the near-surface uncertainties thus cancels out.

The fine spacings are determined predominantly by the sound-speed gradient in the core. Using the asymptotic theory of p -modes it can be shown that (see e.g., Christensen-Dalsgaard & Berthomieu 1991)

$$d_{l,l+2}(n) \simeq -(4l + 6) \frac{\Delta_l(n)}{4\pi^2\nu_{n,l}} \int_0^R \frac{dc}{dr} \frac{dr}{r}, \quad (2)$$

where, R is the solar radius, and $\Delta_l(n)$ is the large frequency spacing given by

$$\Delta_l(n) = \nu_{n,l} - \nu_{n-1,l}, \quad (3)$$

which depends inversely on the sound-travel time between the centre and the surface of the Sun. Given that the gradient of the sound-speed is large in the core, and r there is small, the integral in Eq. 2 is dominated by conditions in the core, and hence the fine spacings are a useful tool to study conditions in the solar core.

Although the difference between the frequencies of two modes that have very similar frequencies does reduce the effect of near-surface uncertainties, there are some residual effects. One way of reducing the effects of the near-surface errors is to use the so-called *frequency separation ratios*. The frequency separation ratios (Roxburgh & Vorontsov 2003; Ot'í Floranes, Christensen-Dalsgaard & Thompson 2005; Roxburgh 2005) are formed from the fine (small) frequency spacings and large frequency spacings of the modes. The ratios are constructed according to:

$$r_{02}(n) = \frac{d_{02}(n)}{\Delta_1(n)}, \quad r_{13}(n) = \frac{d_{13}(n)}{\Delta_0(n+1)}. \quad (4)$$

Since both the small and large spacings are affected in the same manner by near-surface effects, these ratios are somewhat independent of the structure of the surface.

In this paper we use data from BiSON to form observational estimates of the fine spacings, $d_{02}(n)$ and $d_{13}(n)$, and the separation ratios, $r_{02}(n)$ and $r_{13}(n)$. The observed spacings and ratios have then been compared with estimates formed from a number of different solar models. BiSON data on the fine spacings have been used in several previous studies (e.g., Elsworth et al. 1990; Chaplin et al. 1997), but those here come from much longer observations and have far superior precision.

The rest of the paper is organized as follows: the observed data are described in § 2, the solar models are described in § 2.2, we present and explain our results in § 3, and we

discuss the implications of these results to solar neutrino predictions in § 4, and we present our conclusions in § 5.

2. Data

2.1. Observations

We have used Doppler velocity observations made by the BiSON over the 4752-d period beginning 1992 December 31, and ending 2006 January 3. Mode peaks in the power spectrum of the complete time series were fitted in the usual manner (e.g., see Chaplin et al. 1999) to yield estimates of the low- l frequencies.

2.1.1. Impact of the solar cycle on the Sun-as-a-star frequencies

The BiSON observations are examples of the so-called *Sun-as-a-star* data: averages over the visible disc of the perturbations – here, in Doppler velocity – associated with the modes. Chaplin et al. (2005) showed that fine spacings and separation ratios made from the Sun-as-a-star data are sensitive to the changing surface activity along the solar cycle. In short, the acoustic asphericity leaves its imprint on the azimuthally dependent Sun-as-a-star frequencies.

Some of the mode components are effectively missing from the data because the sensitivity of the observations to them is so low. This is a consequence of the visibility of any given m being a strong function of the angle of inclination, i , offered by the star. Extant Sun-as-a-star observations, such as those of the BiSON, are made from $i \approx 90$ degrees. This means that only components with $l + m$ even have non-negligible visibility. As such, it is not possible to estimate directly the frequency centroid; and estimates of the ‘frequency’ of a mode will be influenced strongly by the $|m| = l$ modes, which are most prominent in the data. The Sun-as-a-star fine spacings are therefore formed from modes with different combinations of l and m , which may suffer different sized frequency shifts through the solar cycle.

For the $d_{02}(n)$ data, estimates of the $l = 2$ frequencies are dominated by the $|m| = 2$ modes. They show significantly larger cycle shifts than the lone components of the nearby $l = 0$ modes (e.g., see Chaplin et al. 2004a; Jiménez-Reyes et al. 2004). The $d_{02}(n)$ therefore decrease in size as levels of surface activity increase. Differences between the $|m| = 3$ and 1 components of, respectively, the $l = 3$ and 1 modes, are less pronounced, and so cycle shifts

arising in the $d_{13}(n)$ are smaller, at fixed frequency, than in their $d_{02}(n)$ counterparts.

The separation ratios show a similar behavior. For these data, changes in the large spacing, $\Delta_l(n)$, which lies in the denominator of Equation 4, are negligible. This is because $\Delta_l(n)$ is formed from the difference of two frequency estimates in modes with the same combination of l and m . While it is true that there is a dependence of the mode shifts on frequency, the separation of the overtones used to form the $\Delta_l(n)$ is sufficiently small that the impact of this dependence is modest. Changes to the separation ratios are therefore dominated by changes to the fine spacings. This means that fractional changes in the $r_{02}(n)$ are, to first order, the same as those in the $d_{02}(n)$ [and likewise for the $r_{13}(n)$ and $d_{13}(n)$].

2.1.2. Correction of the Sun-as-a-star frequencies for the solar cycle

Prior to calculation of the fine spacings and separation ratios, we therefore removed the solar-cycle shifts from the raw fitted low- l frequencies. Our procedure rests on the assumption that variations in certain global solar activity indices can be used as a proxy for the low- l frequency shifts, $d\nu_{n\ell}(t)$. We assume the correction can be parameterized as a linear function of the chosen activity measure, $A(t)$. When the 10.7-cm radio flux (Tapping & De Tracey 1990) is chosen as the proxy, this assumption is found to be robust (e.g., Chaplin et al. 2004a) at the level of precision of the data.

Consider then the set of measured eigenfrequencies, $\nu_{n\ell}(t)$, that we wish to correct, extracted from data collected over the $t = 4752$ d epoch when the mean level of the 10.7-cm radio flux was $\langle A(t) \rangle = 121 \times 10^{-22} \text{ W m}^{-2} \text{ Hz}^{-1}$. We make the correction to the canonical quiet-Sun level of the radio flux, A_{quiet} , which, from historical observations of the index, is usually fixed at $64 \times 10^{-22} \text{ W m}^{-2} \text{ Hz}^{-1}$ (see Tapping & DeTracey 1990). The magnitude of the solar-cycle correction – which must be subtracted from the raw frequencies – will then be:

$$\delta\nu_{n\ell}(t) = g_\ell \cdot \mathcal{F}[\nu] \cdot [\langle A(t) \rangle - A_{\text{quiet}}]. \quad (5)$$

The g_ℓ are l -dependent factors that calibrate the size of the shift: recall from Section 2.1.1 above that the Sun-as-a-star shifts alter significantly with l . Owing to the nature of the Sun-as-a-star data, the change with l comes from the spatial dependence of the surface activity. To determine the g_ℓ , we divided the 4752-day timeseries into 44 independent 108-day segments. The resulting ensemble was then analyzed, in the manner described by Chaplin et al. (2004a), to uncover the dependence of the solar-cycle frequency shifts on the 10.7-cm radio flux. The $\mathcal{F}[\nu]$ in Equation 5 is a function that allows for the dependence of the shift on mode frequency. Here, we used the determination of $\mathcal{F}[\nu]$ to be found in Chaplin et al. (2004a, b).

Uncertainty in the correction is dominated by the errors on the g_l . These errors must be propagated, together with the formal uncertainties from the mode fitting procedure, to give uncertainties on the corrected frequencies, $\nu_{n\ell}(t) - \delta\nu_{n\ell}(t)$. The corrected uncertainties are, on average, about 10% larger than those in the raw, fitted frequencies.

After application of the correction procedure, fine spacings and separation ratios were calculated according to Equations 1 and 4 respectively. Uncertainties on the corrected frequencies were propagated accordingly to give those in the spacings and ratios.

Fig. 1 shows the differences between fine spacings made with and without the correction (in the sense corrected spacings minus raw spacings). The ratio data give similar-looking plots. As indicated previously, it is the $d_{02}(n)$ (and by implication the $r_{02}(n)$) that are most affected by the correction procedure.

2.2. Models

For the major part of the work we used eight solar models that have been constructed with different physical inputs. The models are:

JCDS — Model S of Christensen-Dalsgaard et al. (1996). This model was constructed with surface $Z/X = 0.0245$ (Grevesse & Noels 1993), OPAL(1992) opacities (Rogers & Iglesias 1992) and the OPAL(1996) equation of state (Rogers, Swenson & Iglesias 1996). This model was used because many helioseismological results in literature are based on this reference model.

SAC — Model Seismic₁ of Couvidat et al. (2003). It used OPAL(1996) opacity tables (Iglesias and Rogers 1996), and the OPAL(1996) equation of state (Rogers, Swenson & Iglesias 1996). The model has $(Z/X) = 0.02628$.

BP04 – Model BP04(Garching) of Bahcall et al. (2005c). This model was constructed with GS abundances ($Z/X = 0.0229$), OPAL(1995) opacities (Iglesias & Rogers 1996) and the OPAL(2001) equation of state (Rogers 2001, Rogers & Nayfonov 2002).

BP04+ — Model BP04+ of Bahcall et al. (2005a). This model was constructed with abundances from Asplund et al. (2000, 2004), Asplund (2000), Allende Prieto et al. (2001, 2002). These abundances imply $Z/X = 0.0176$ as opposed to the $Z/X = 0.0229$ of GS. Only abundances of C, N, O, Ne and Ar are lowered in comparison to model BP04. The rest of the input physics is the same as BP04.

BS05(OP) — Model BS05(OP) of Bahcall et al. (2005c). This model is similar to model

BP04, but has been constructed with opacities from the OP project (Badnell et al. 2005) instead of the OPAL opacities. There are some other subtle differences too, such as in the treatment of diffusion where, unlike in BP04, each metal has a different diffusion velocity as derived from Thoul et al. (1993). Also, unlike in BP04, ^{17}O is not burned at all. The model was constructed with GS abundances and has a surface $Z/X = 0.02292$.

BS05(AGS, OP) — Model BS05(AGS, OP) of Bahcall et al. (2005c). This model is similar to model BS05(OP), and was constructed with AGS abundances, having surface $Z/X = 0.01655$.

BBS05-3 — Model 3 of Bahcall et al. (2005b). This model has the same physics as BS05(OP) and BS05(AGS, OP), but the Ne, Ar, CNO and Si abundances have been enhanced with respect to the AGS values. The model has $Z/X = 0.02069$.

S06+(AGS, OP) — A model constructed specifically for this work. It is similar to model BS05(AGS, OP), however, the opacities have been artificially increased by 13% in the temperature range of 2 to 5 million Kelvin to get the helioseismically determined position of the convection-zone base.

We also used three other models to test the effect of heavy elements, keeping all other input physics the same. These models were constructed using YREC, the Yale Rotating Evolution Code, in its non-rotating configuration (Guenther et al. 1992). All models have the same physics inputs except the heavy-element abundances. The models use the OPAL2001 equation of state, and OPAL(1996) opacities. The models are:

YREC(AGS) — model with surface $Z/X = 0.0165$, the AGS value of surface metallicity.

YREC(GS) — model with surface $Z/X = 0.0229$, the GS value of surface metallicity.

YREC(0.03) — model with a high metallicity, $Z/X = 0.03$, constructed to check if the effect of metallicity is monotonic.

All models except S06+(AGS, OP) and the three YREC models are published models. The models have been calibrated to slightly different values of luminosity and radius. The SAC model has a radius of 6.95936×10^{10} cm. All others have a radius of 6.9598×10^{10} cm. Model JCDS has a luminosity of 3.8456×10^{33} ergs/s; models BP04, BP04+, BS05(OP), BS05(AGS, OP), BBS05-3, and S06+(AGS, OP) have luminosities of 3.8418×10^{33} ergs/s; and the three YREC models have a luminosity of 3.851×10^{33} ergs/s. The luminosity that the SAC model was calibrated to has not been published.

The frequencies for each of these models was calculated by solving the full set of equations describing stellar oscillations. The numerical precision of the frequencies was increased

using the Richardson extrapolation technique. Once the frequencies were calculated, The large and small separations, and the separation ratios were calculated using equations 1, 3, and 4.

3. Results and Discussion

Each panel of Fig. 2 shows the fine spacings, $d_{02}(n)$, from one of the solar models. Model data are rendered as a solid line, and the models are identified in the plot titles. The panels also show for direct comparison the $d_{02}(n)$ calculated from the corrected BiSON frequencies (points with error bars). Figs. 3, 4 and 5 show similar plots for the $d_{13}(n)$, $r_{02}(n)$ and $r_{13}(n)$ data respectively.

The fine spacings and separation ratios show a marked dependence on mode frequency. Removal of these trends allows for a more detailed visual comparison of differences between the BiSON and model data. In the case of the fine spacings, we have followed an approach similar to that given in Chaplin et al. (1997). Here, a simple linear model of the form

$$d_{l+2}(n) = c_0 + c_1\nu \tag{6}$$

was fitted to each set of BiSON fine spacings. The Fit to the $d_{02}(n)$ data, made over the range ~ 1408 to $\sim 3985 \mu\text{Hz}$, gave best-fitting coefficients of $c_0 = 15.95 \pm 0.06 \mu\text{Hz}$ and $c_1 = (-2.24 \pm 0.02) \times 10^{-3}$; while the fit to the $d_{13}(n)$ data, made over the range ~ 1473 to $\sim 3640 \mu\text{Hz}$, gave coefficients $c_0 = 26.29 \pm 0.20 \mu\text{Hz}$ and $c_1 = (-3.35 \pm 0.08) \times 10^{-3}$. The best-fitting models were then subtracted from the BiSON spacings, and each set of model spacings, to yield the residuals that are plotted in the two panels of Figs. 6 (see caption for details). By adopting this approach of characterizing the spacings by a simple linear model we preserve in the residuals various features in frequency that are common to both the observations and models. The feature around $\sim 2000 \mu\text{Hz}$ which is present in the various curves in Fig. 6 is the signature of the HeII ionization zone. The presence of this feature in the data shows that the fine-spacings are not immune to the near-surface structure.

The separation ratios $r_{02}(n)$ in contrast show marked departures from linear behavior with frequency at the low-overtone end of the plotted data. Furthermore, these data, and the $r_{13}(n)$, tend to vary more smoothly in frequency than do their fine-spacing counterparts. In Fig. 7 we therefore plot just the differences between the observed and model ratios (see caption for details).

Tables 1 and 2 give quantitative measures of the differences between the observed and model datasets. Table 1 shows weighted mean differences (in the sense BiSON minus model),

and weighted RMS differences, for the fine spacing data (all in μHz). The formal uncertainties on the BiSON spacings were used to fix the weights (with the usual uncertainty-squared Gaussian weighting applied), and to calculate an internal error on each mean or RMS difference. Significance levels for the differences (in units of sigma) appear in the table in brackets, and were computed by dividing each mean or RMS difference by its associated internal error.

Table 2 shows similar data for the separation ratios. Here, the mean differences are weighted *fractional* differences between the BiSON and model values. Because each ratio is formed from the quotient of two separations in frequency, with the uncertainties on these separations assumed to follow Gaussian distributions, determination of the fractional differences allows errors to be given that are also Gaussian (and not asymmetric) in the final measure.

From inspection of the various figures, particularly Figs. 6 and 7, and the data in the two tables, it is apparent immediately that the models that show the poorest correspondence with the observations are those that have lowered abundances, i.e., models BP04+, BP05(AGS,OP) and S06+(AGS,OP). Model BP04+ has slightly higher metallicity than models BP05(AGS,OP) and S06+(AGS,OP), and so fares slightly better in the comparisons. The models with higher abundances do much better: model JCDS, although constructed with outdated inputs, agrees quite well with the observations, as do models BP04 and BS05(OP). The non-standard model, BBS05-3, does well too. Model SAC does not fare as well as models JCDS or BP04, however, it still agrees better than do the models with lower abundances. Thus we can say the models with lower than GS abundances have core structures that do not match that of the Sun.

We shall not discuss models JCDS and SAC further, except to note again that they fare much better than the low- Z/X models. Models JCDS and SAC were constructed using the older OPAL equation of state, which did not treat relativistic effects at temperatures and densities relevant to the solar core. This resulted in a somewhat deficient core structure (see Elliot & Kosovichev, 1998). We shall discuss in more detail below results obtained from models that were instead constructed with the *corrected* OPAL equation of state.

Model S06+(AGS, OP) was made because a localized change in opacities can resolve the problem of the convection zone depth in models with AGS abundances (see, e.g. Basu & Antia 2004; Bahcall et al. 2005a). However, it is very clear from the fine spacings, and separation ratios that this model fails in the core.

We find that the model BBS05-3 does reasonably. This model was constructed by increasing the amount of neon compared to the AGS abundances, in addition to increasing the quantities of some of the other elements. A strategy of increasing the amounts of neon

and other elements (within their error bars) was suggested by Antia & Basu (2005) and Bahcall et al. (2005) as a potential way to solve the disagreement between the helioseismic observations and the models with AGS abundances. Neon contributes to the opacity near the convection-zone base. An increase in the neon abundance therefore deepens the convection zone, bringing the models into agreement with the helioseismically determined convection-zone depth. It is worth adding that because of the abundance increases in some of the elements this model has a relatively high Z/X (0.02069).

Differences between the results of the various models ultimately have to be understood in terms of the sound-speed gradient in the core which, *as per* Eq. 2, determines the fine spacings and therefore also the separation ratios. Sound speed is determined both by temperature T and mean molecular weight μ , with $c^2 \propto T/\mu$. The gradient of sound speed is therefore determined by the gradients of temperature and μ as well. Although the sound-speed gradient is negative in the bulk of the Sun, it is positive at very small radii because of the different radial dependences of T and μ , with the increase in μ at smaller r compensating the increasing T to give a lower c .

We can use the three YREC models to determine why the other models with lower metallicity fare worse than models with higher metallicity in comparison with the BiSON data. Fig. 8 shows the fine spacings and separation ratios of the YREC models, together with the BiSON data (points with error bars). We can see that increasing the surface Z/X decreases the fine spacings and separation ratios. To explain these results we show in Fig. 9 the sound-speed gradient and the mean molecular weight profiles of the YREC models. It is clear that differences between the models lie very close to the center, where dc/dr is positive. A more detailed analysis of the structure of the YREC models shows that the $-\sqrt{T/\mu^3} (d\mu/dr)$ term in the sound-speed gradient is instrumental in causing the differences, in particular the factor $\sqrt{1/\mu^3}$. The models have very similar temperatures, temperature gradients and μ gradients, but the larger μ in models with higher Z/X increases dc/dr in the core, thereby decreasing the value of the integral in Eq. 2.

The μ dependence of the sound-speed gradient explains why models BP04+ and BBS05-3 do not behave like BS05(AGS, OP) and S06+(AGS,OP). Model BP04+ does not have as low metallicities as BS05(AGS, OP) and S06+(AGS,OP) and hence fares better than these models. That said, the metallicity of BP04+ is low enough to give larger fine spacings and separation ratios than are seen in the GS models.

Model S06+(AGS, OP) does not do well in the core, despite satisfying the helioseismic constraints at the base of the convection zone, because μ in its core remains similar to that in model BS05(AGS, OP). The change in opacity in S06+(AGS, OP) does however induce changes in the rest of the model (solar structure is, after all, determined by a set of highly

coupled equations), and this causes enough difference in the core temperature gradient to give different fine spacings and separation ratios compared with BS05(AGS, OP).

This leads us to the question of the differences in the spacings and ratios of models BP04 and BS05(OP). That there are differences is not surprising because even though they have the same metallicity, the models were constructed with slightly different opacities. The temperature gradient in the radiative zone (and that includes the solar core) is determined by the opacity, and hence different opacities will imply a different temperature gradient. Differences in the treatment of diffusion and ^{17}O burning also have a small effect because both change the μ gradient slightly. Nonetheless, the overall opacity differences in the models lead to only modest differences in the fine spacings and separation ratios.

From the above discussion it is clear that models with low metallicities, such as those with AGS abundances, do not satisfy the observational constraints imposed by the BiSON fine-spacing and separation-ratio data. Though subtle changes in physics (such as in the formulation of diffusion, etc.) do change the core structure, the changes are sufficiently small to allow us to distinguish between the GS and AGS abundances. In fact, looking at Fig. 8, we might be tempted to determine the solar metallicity using the fine spacings and separation ratios.

4. Implications for neutrino uncertainties

Uncertainties in solar neutrino predictions arise from uncertainties in inputs to the solar models. It has, however, been long recognized that the predominant source of uncertainty is the composition (Sears 1964, Bahcall 1966). As a result there has been a large body of work devoted to evaluating neutrino uncertainties, among the more recent being Fiorentini & Ricci (2002), Couvidat et al. (2003), Boothroyd & Sackmann (2003), Bahcall & Pinsonneault (2004), Young & Arnett (2005), Bahcall & Serenelli (2005), and Bahcall et al. (2006).

Bahcall & Serenelli (2005) performed a very detailed and rigorous investigation of how the abundances of individual elements affect solar neutrino predictions. Their study was motivated by the fact that models with AGS abundances show discrepancies with respect to the Sun just below the solar convection zone. Bahcall & Serenelli (2005) found that the largest uncertainties in the ^7Be and ^8B neutrinos are due to the uncertainty of the solar iron abundance. However, uncertainties in oxygen, neon, silicon and sulphur also contribute significantly to the ^7Be and ^8B flux uncertainties. The p-p neutrino flux is most sensitive to changes in the iron abundance, but because carbon uncertainties are larger, both elements dominate and contribute comparable amounts to the total uncertainty. It should be noted

that the 8B neutrinos are the ones detected by the water (Kamiokande & Superkamiokande) and heavy-water detectors (Sudbury Neutrino Observatory). 8B , 7Be and pep neutrinos are detected by Chlorine detectors. In order to calculate the uncertainty, Bahcall & Serenelli (2005) adopted what they called a “conservative” uncertainty in the abundances. This uncertainty is basically the difference between the GS and AGS abundance values. Their so-called “optimistic” uncertainty was based on the error bars on the abundance from the AGS table. The “conservative” uncertainties are much larger than the “optimistic” uncertainties. It should be noted that quoted uncertainties in the GS and AGS tables are fairly similar. Work done by Bahcall et al. (2006) confirmed these results through an elaborate Monte-Carlo simulation.

Our current work has shown that models with AGS abundances fare much worse than models with GS abundances. We also see, from Fig. 8, that the uncertainties in the abundances are probably much less than the difference between the GS and AGS values. We therefore conclude that the “conservative” uncertainties in the neutrino fluxes are unduly pessimistic and can be lowered substantially. Not having done the full analysis, we are unable to say if we are justified in lowering the levels to the “optimistic” levels of Bahcall & Serenelli (2005) and Bahcall et al. (2006).

Our conclusion however comes with one condition, which is related to the model with modified neon abundance (BBS05-3) and the fact it did well in comparisons with the BiSON data. The solar neon abundance is very uncertain since the abundance cannot be measured at the photosphere. This had led Antia & Basu (2005) and Bahcall et al. (2005b) to propose increasing the neon abundance as a solution to the helioseismic problems posed by the AGS models. Drake & Testa (2005) found that most neighboring stars seem to have a much higher Ne/O ratio compared to the Sun, which supported increasing the neon abundance. However, Schmelz et al. (2005) and Young (2005) each reanalyzed solar X-ray and UV data and found that the Ne/O ratio of the Sun is indeed low. Bochsler et al. (2006) also suggest a low solar Ne/O abundance. A more detailed analysis of the convection zone also points to the fact that an enhanced neon abundance will not reconcile models with the helioseismic data (Basu & Antia 2006). Thus although the neon issue has not been resolved completely, it looks increasingly unlikely that the solar neon to oxygen ratio is high. We are therefore reasonably confident about our claim that uncertainties in the predicted solar neutrino fluxes can be lowered.

5. Conclusions

We have used BiSON data collected over 4752 days to determine the frequencies of low-degree acoustic solar oscillation modes. These frequencies have been used to calculate the fine or small frequency spacings and frequency separation ratios for the Sun. These spacings and ratios have then been used to test different solar models to investigate whether or not we can constrain solar abundances.

We find that models constructed with the older Grevesse & Sauval (1998) mixture satisfy the fine-spacing and separation-ratio constraints much better than do models with the newer Asplund et al. (2005) abundances. In fact, models with high metallicity constructed with outdated opacities and equation-of-state data also fare better than do the recent models with Asplund et al. (2005) abundances. Our investigation shows that the fine spacings and separation ratios depend sensitively on the metallicity, and low-metallicity models can be ruled out.

Our results lead us to conclude that uncertainties on predicted solar neutrinos, which had been raised because of the Asplund et al. (2005) abundances, can now be lowered.

This paper utilizes data collected by the Birmingham Solar-Oscillations Network (BiSON), which is funded by the UK Particle Physics and Astronomy Research Council (PPARC). We thank the members of the BiSON team, colleagues at our host institutes, and all others, past and present, who have been associated with BiSON. GAV acknowledges the support of PPARC. The radio flux observations are made at Penticton by the National Research Council of Canada and are available from the World Data Center. SB acknowledges partial support from NSF grant ATM-0348837. She would also like to thank the BiSON group for their hospitality during the time this work was carried out. AMS is partially supported by the NSF (grant PHY-0503684), the Association of Members of the Institute for Advanced Study and the W. M. Keck Foundation through a grant-in-aid to the Institute for Advanced Study.

REFERENCES

- Allende Prieto, C., Lambert, D. L., & Asplund, M. 2001, *ApJ*, 556, L63
- Allende Prieto, C., Lambert, D. L., & Asplund, M. 2002, *ApJ*, 573, L137
- Antia, H.M. & Basu, S. 2005, *ApJ*, 620, L129

- Antia, H.M., Basu, S. 2006, ApJ, 644, 1292
- Asplund, M. 2000, A&A, 359, 755
- Asplund, M., Grevesse, N., Sauval, A. J., Allende Prieto, C., & Kiselman, D. 2004, A&A, 417, 75
- Asplund, M., Nordlund, A., Trampedach, R., & Stein, R. F. 2000, A&A, 359, 743
- Asplund, M., Grevesse, N., & Sauval, A. J. 2005, in Cosmic abundances as records of stellar evolution and nucleosynthesis, eds. F. N. Bash & T. G. Barnes, ASP Conf. Series, vol. 336, 25
- Asplund, M., Grevesse, N., Sauval, A. J., Allende Prieto, C., Blomme, R., 2005, A&A, 431, 693
- Badnell, N. R., Bautista, M. A., Butler, K., Delahaye, F., Mendoza, C., Palmeri, P., Zeippen, C. J., & Seaton, M. J. 2005, MNRAS, 360, 458
- Bahcall, J.N. 1964, Phys. Rev. Lett., 12, 300
- Bahcall, J.N., Pinsonneault, M.H. 2004, Phys. Rev. Lett., 92, 121301
- Bahcall, J.N., Serenelli, A.M. 2005, ApJ, 626, 530
- Bahcall, J.N., Huebner, W.F., Lubow, S.H., Parker, P.D., Ulrich, R.K. 1982, Rev. Mod. Phys., 54, 767
- Bahcall, J.N., Pinsonneault, M.H., Basu, S., Christensen-Dalsgaard, J. 1997, Phys. Rev. Lett., 78, 171
- Bahcall, J. N., Basu, S., Pinsonneault, M. H., & Serenelli, A. M. 2005a, ApJ, 618, 1049
- Bahcall, J. N., Basu, S., Serenelli, A.M. 2005b, 631, 1281
- Bahcall, J. N., Serenelli, A. M., & Basu, S. 2005c, ApJ, 621, L85
- Bahcall, J. N., Serenelli, A. M., & Basu, S. 2006, ApJS, 165, 400
- Balmforth, N. J. 1992, MNRAS, 255, 632
- Basu, S., & Antia, H. M. 2004, ApJ, 606, L85
- Basu, S., Antia H.M. 2006, in proc. SOHO17: 10 years of SOHO and beyond, ESA SP-617, eds. D. Spadaro, B. Fleck & J.B. Gurman, in press

- Basu, S., Pinsonneault, M.H., Bahcall, J.N. 2000, *ApJ*, 529, 1084
- Boothroyd, A.L., Sackmann, I.J., 2003, *ApJ*, 583, 1004
- Bochsler, P., Auchère, F., Skoug, R.M. 2006, in *proc. SOHO17: 10 years of SOHO and beyond*, ESA SP-617, eds. D. Spadaro, B. Fleck & J.B. Gurman, in press
- Couvidat, S., Turck-Chieze, S., Kosovichev, A.G. 2003, *ApJ*, 599, 1434
- Chaplin W. J., Elsworth Y., Howe R., Isaak G. R., McLeod C. P., Miller B. A., New R., van der Raay H. B. & Wheeler S. J., 1996, *Sol. Phys.*, 168, 1
- Chaplin W. J., Elsworth Y., Isaak G. R., McLeod C. P., Miller B. A., New R., 1997, *ApJ*, 480, L75
- Chaplin W. J., Elsworth Y., Isaak G. R., Miller B. A., New R., 1999, *MNRAS*, 308, 424
- Chaplin W. J., Elsworth Y., Isaak G. R., Miller B. A., New R., 2004a, *MNRAS*, 352, 1102
- Chaplin W. J., Appourchaux T., Elsworth Y., Isaak G. R., Miller B. A., New R., Toutain T., 2004b, *A&A*, 416, 341
- Chaplin W. J., Elsworth Y., Miller B. A., New R., Verner G. A., 2005, *ApJ*, 635, L105
- Christensen-Dalsgaard, J. 2003, *Rev. Mod. Phys.*, 74, 1073
- Christensen-Dalsgaard, J., Berthomieu, G. 1991, in *Solar Interior and Atmosphere*, eds. A.N. Cox, W.C.Livingston, M.S. Matthews, University of Arizona Press, Tucson, p401
- Christensen-Dalsgaard, J., Däppen, W., Ajukov, S.V., et al. 1996, *Science*, 272, 1286
- Cox, A. N., & Kidman, R. B. 1984, in *Theoretical problems in stellar stability and oscillations* (Liège: Institut d'Astrophysique), 259
- Delahaye, F., & Pinsonneault M. H. 2005, [astro-ph/0511779](https://arxiv.org/abs/astro-ph/0511779)
- Drake, J.J., & Testa, P. 2005, *Nature*, 436, 525
- Elliott, J.R., Kosovichev, A.G. 1998, *ApJ*, 500, L199
- Elsworth Y., Howe R., Isaak G. R., McLeod C. P., New R., 1990, *Nature*, 347, 536
- Fiorentini, G., Ricci, B. 2002, *Phys. Lett. B.*, 526, 186
- Grevesse, N., & Noels, A. 1993, in *Origin and evolution of the Elements*, ed. N. Prantzos, E. Vangioni-Flam, & M. Cassé (Cambridge: Cambridge Univ. Press), 15

- Grevesse, N., & Sauval, A. J. 1998, in *Solar composition and its evolution — from core to corona*, eds., C. Fröhlich, M. C. E. Huber, S. K. Solanki, & R. von Steiger, Kluwer, Dordrecht, p. 161
- Guenther, D. B., Demarque, P., Kim, Y.-C., Pinsonneault, M. H. 1992, *ApJ*, 387, 372
- Iglesias, C. A., & Rogers, F. J. 1996, *ApJ*, 464, 943
- Jiménez-Reyes S. J, García R. A., Chaplin W. J., Korzennik S. G., 2004, *ApJ*, 610, L65
- Morel, P., Pinchon, B., Provost, J., Berthomieu, G. 1999, *A&A*, 350, 275
- Otí Floranes H., Christensen-Dalsgaard J., Thompson M. J., 2005, *MNRAS*, 356, 671
- Pinsonneault, M.H., Delahaye, F. 2006, *astro-ph/0606077*
- Rogers, F.J., Iglesias, C.A. 1992, *ApJ*, 401, 361
- Rogers, F. J. 2001, *Contrib. Plasma Phys.*, 41, 179
- Rogers, F. J., Swenson, F. J., & Iglesias, C. A. 1996, *ApJ*, 456, 902
- Rogers, F. J., & Nayfonov, A. 2002, *ApJ*, 576, 1064
- Roxburgh I. W., Vorontsov S. V., 2003, *A&A*, 411, 215
- Roxburgh I. W., 2005, *A&A*, 434, 665
- Schmelz, J.T., Nasraoui, K., Roames, J.K., Lippner, L.A., Garst, J.W. 2005, *ApJ* 634, L197
- Sears, R.L. 1964, *ApJ*, 140, 477
- Tapping K. F., DeTracey B., 1990, *Sol Phys*, 127, 321
- Thoul, A. A., Bahcall, J. N., & Loeb, A. 1994, *ApJ*, 421, 828
- Young, P.R. 2005, *A&A* 444, L45
- Young, P.A., Arnett, D. 2005, *ApJ*, 618, 908

Table 1. Difference in fine-structure spacings (BiSON minus models)

Model	$d_{02}(n)$		$d_{13}(n)$	
	Weighted mean difference (μHz)	Weighted RMS (μHz)	Weighted mean difference (μHz)	Weighted RMS (μHz)
JCDS	−0.058 (−10.8 σ)	0.072 (13.3 σ)	−0.033 (−4.5 σ)	0.053 (7.2 σ)
SAC	−0.133 (−24.7 σ)	0.139 (25.9 σ)	−0.083 (−11.2 σ)	0.094 (12.8 σ)
BP04	−0.009 (−1.7 σ)	0.047 (8.7 σ)	−0.043 (−5.8 σ)	0.091 (12.3 σ)
BP04+	−0.102 (−18.9 σ)	0.126 (23.4 σ)	−0.204 (−27.7 σ)	0.237 (32.2 σ)
BS05(OP)	−0.051 (−9.5 σ)	0.065 (12.0 σ)	−0.083 (−11.3 σ)	0.114 (15.5 σ)
BS05(AGS,OP)	−0.230 (−42.6 σ)	0.243 (45.1 σ)	−0.360 (−48.7 σ)	0.382 (51.7 σ)
BBS05-3	−0.034 (−6.2 σ)	0.063 (11.7 σ)	−0.078 (−10.5 σ)	0.136 (18.4 σ)
S06+(AGS,OP)	−0.145 (−27.0 σ)	0.160 (29.7 σ)	−0.200 (−27.1 σ)	0.267 (36.2 σ)

Table 2. Difference in frequency separation ratios (BiSON minus models)

Model	$r_{02}(n)$		$r_{13}(n)$	
	Weighted mean difference (%)	Weighted RMS (%)	Weighted mean difference (%)	Weighted RMS (%)
JCDS	−0.43 (−9.5 σ)	0.63 (13.7 σ)	−0.03 (−0.8 σ)	0.23 (5.9 σ)
SAC	−0.99 (−21.6 σ)	1.08 (23.5 σ)	−0.22 (−5.6 σ)	0.29 (7.5 σ)
BP04	+0.03 (+0.6 σ)	0.26 (5.7 σ)	+0.02 (+0.4 σ)	0.17 (4.5 σ)
BP04+	−0.85 (−18.6 σ)	0.92 (20.0 σ)	−0.84 (−22.1 σ)	0.89 (23.2 σ)
BS05(OP)	−0.39 (−8.5 σ)	0.46 (10.0 σ)	−0.29 (−7.5 σ)	0.35 (9.2 σ)
BS05(AGS,OP)	−2.02 (−43.9 σ)	2.06 (44.8 σ)	−1.76 (−45.8 σ)	1.80 (46.9 σ)
BBS05-3	−0.05 (−1.1 σ)	0.27 (5.9 σ)	+0.02 (+0.4 σ)	0.22 (5.7 σ)
S06+(AGS,OP)	−0.98 (−21.3 σ)	1.04 (22.5 σ)	−0.58 (−15.1 σ)	0.79 (20.6 σ)

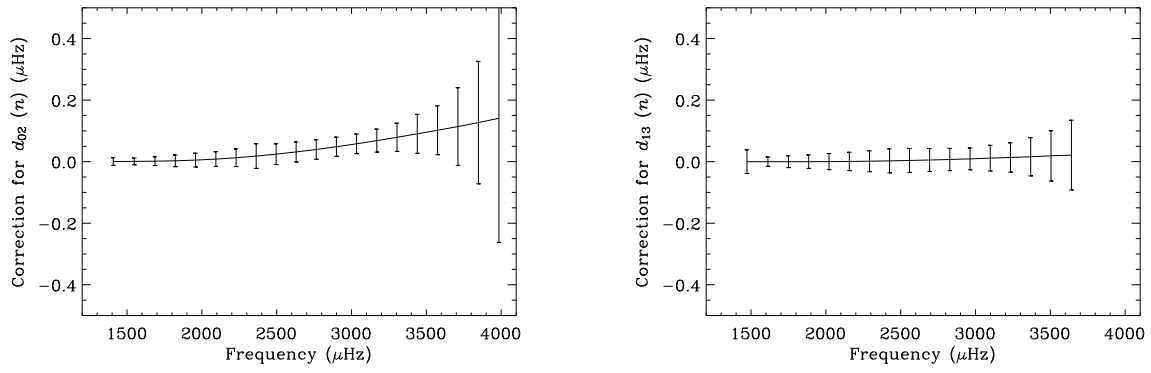


Fig. 1.— Differences between fine spacings made with and without the solar-cycle correction (in the sense corrected spacings minus raw spacings). Left-hand panel: difference/correction in $d_{02}(n)$. Right-hand panel: difference/correction in $d_{13}(n)$.

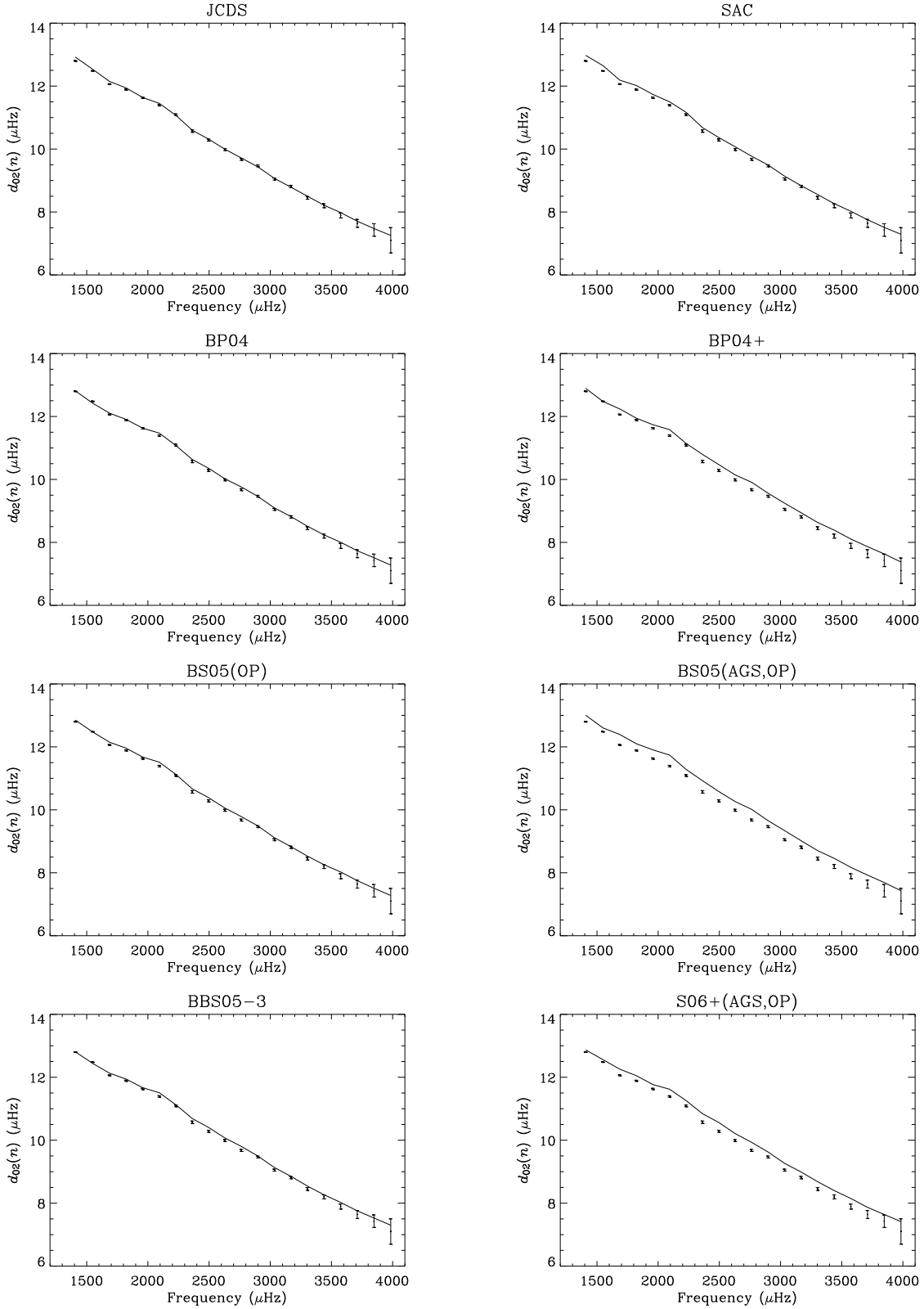


Fig. 2.— Solid line in each panel: fine spacings $d_{02}(n)$ of solar model identified in plot title. Points with error bars: $d_{02}(n)$ from the corrected BiSON frequencies.

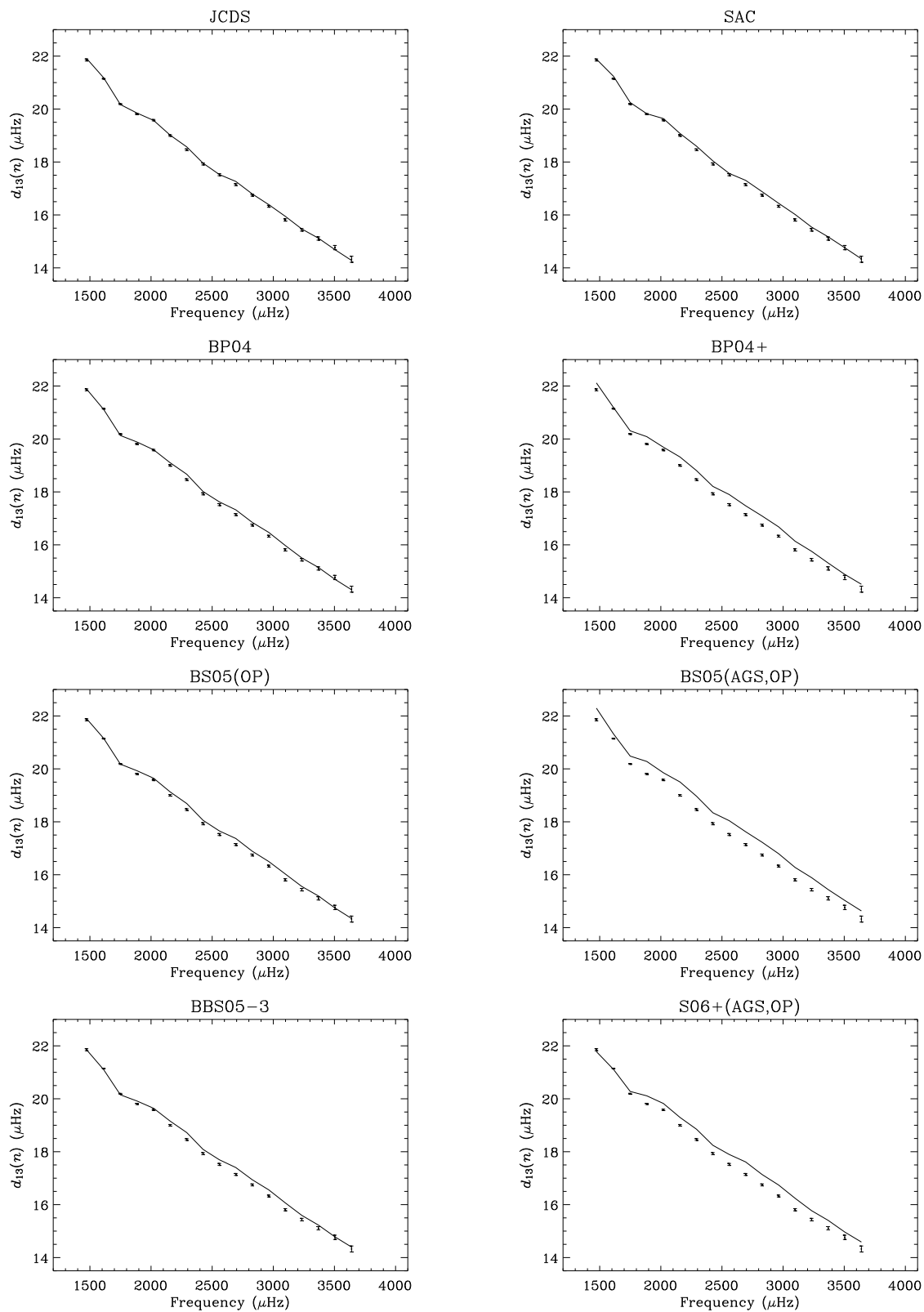


Fig. 3.— Solid line in each panel: fine spacings $d_{13}(n)$ of solar model identified in plot title. Points with error bars: $d_{13}(n)$ from the corrected BiSON frequencies.

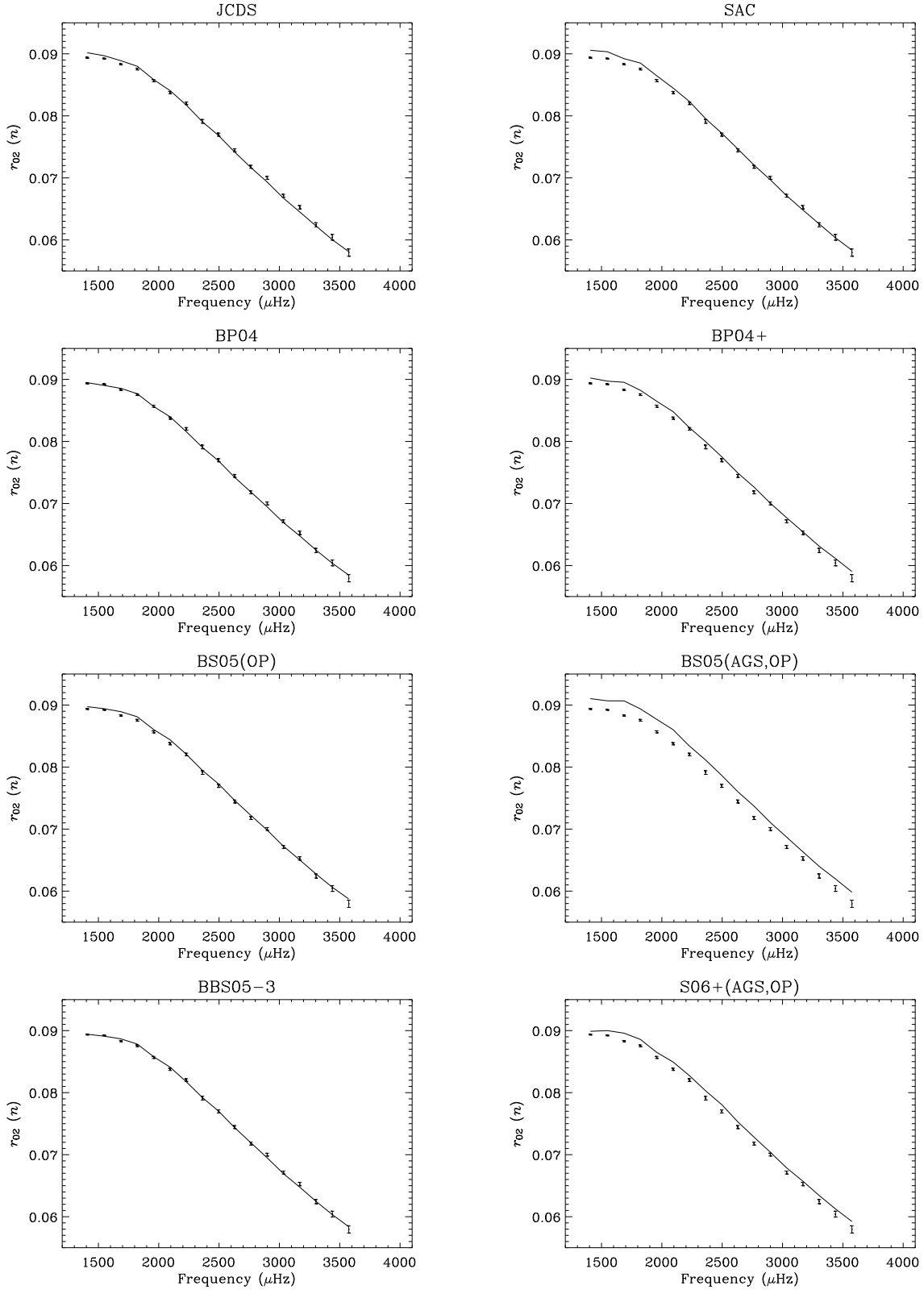


Fig. 4.— Solid line in each panel: separation ratios $r_{02}(n)$ of solar model identified in plot title. Points with error bars: $r_{02}(n)$ from the corrected BiSON frequencies.

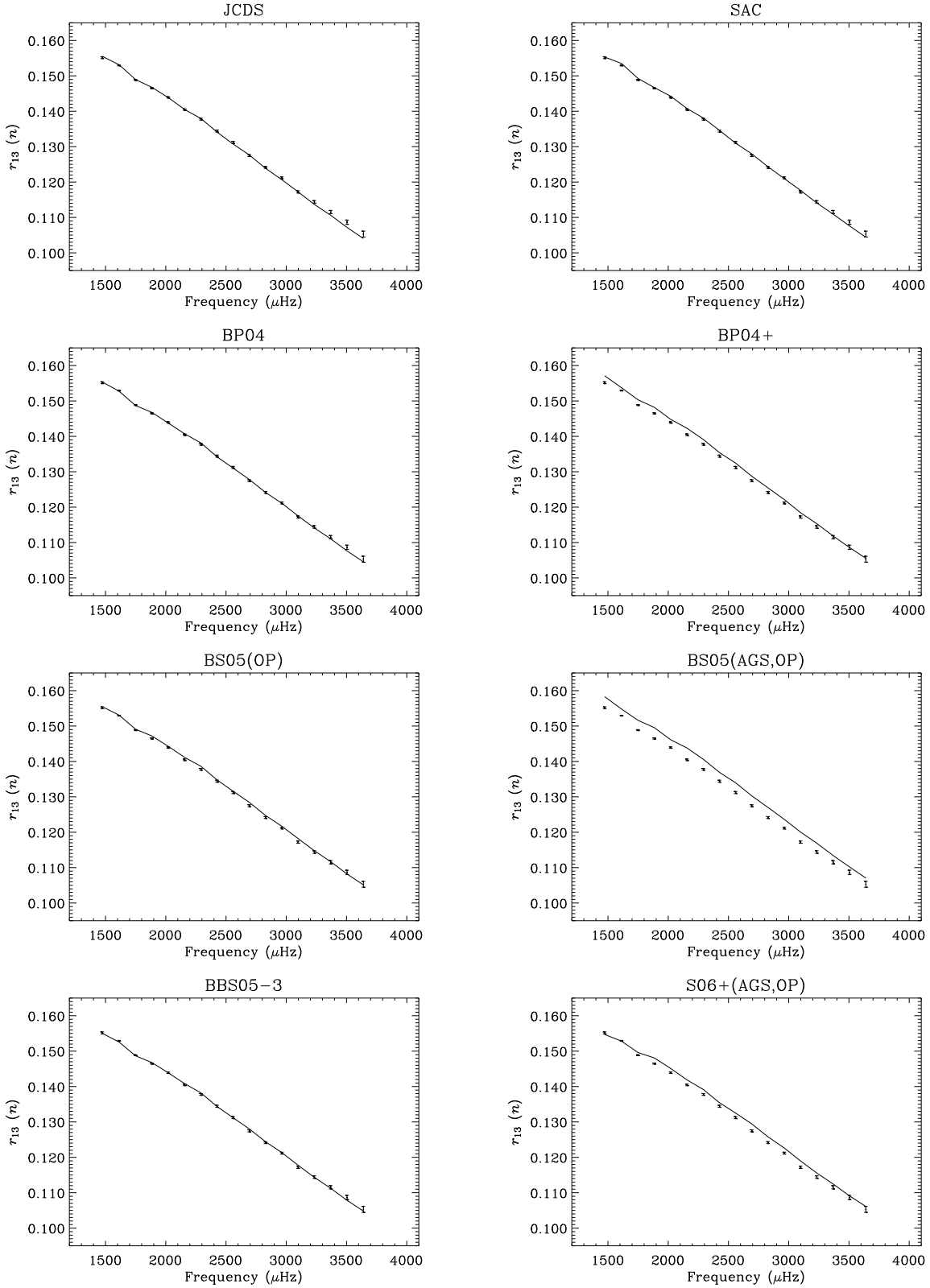


Fig. 5.— Solid line in each panel: separation ratios $r_{13}(n)$ of solar model identified in plot title. Points with error bars: $r_{13}(n)$ from the corrected BiSON frequencies.

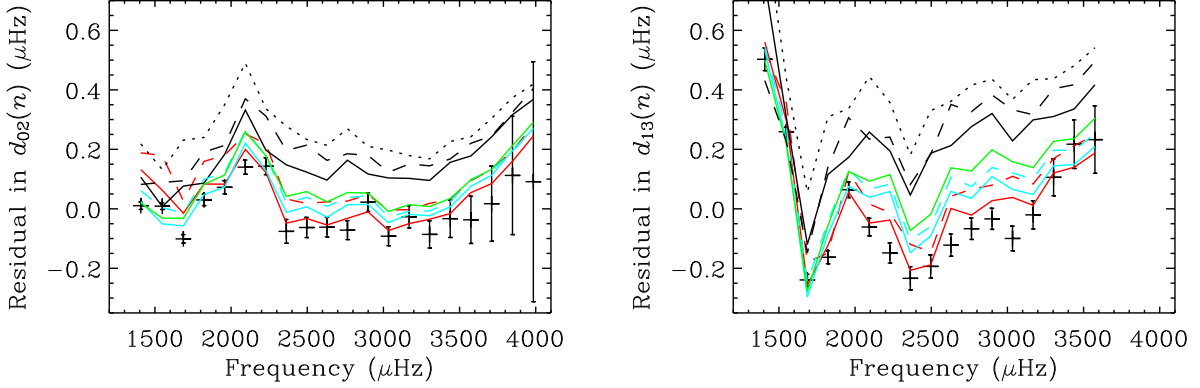


Fig. 6.— Residuals given by subtraction of best-fit straight line (to fine spacings versus frequency) from BiSON fine spacings and each set of model fine spacings. Left-hand panel: residuals in $d_{02}(n)$. Right-hand panel: residuals in $d_{13}(n)$. BiSON data are plotted with their associated error bars. Various models rendered as follows: JCDS (red, solid); SAC (red, dashed); BP04 (cyan, solid); BP04+ (black, solid); BS05(OP) (cyan, dashed); BS05(AGS,OP) (black, dotted); BBS05-3 (green); S06+(AGS,OP) (black, dashed).

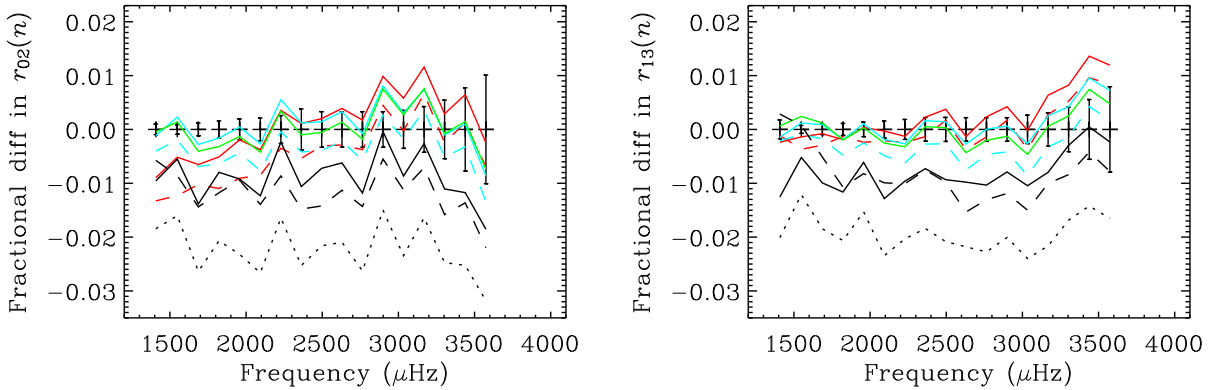


Fig. 7.— Differences between observed BiSON and model separation ratios (in sense BiSON minus model). Left-hand panel: differences in $r_{02}(n)$. Right-hand panel: differences in $r_{13}(n)$. Various models rendered as follows: JCDS (red, solid); SAC (red, dashed); BP04 (cyan, solid); BP04+ (black, solid); BS05(OP) (cyan, dashed); BS05(AGS,OP) (black, dotted); BBS05-3 (green); S06+(AGS,OP) (black, dashed).

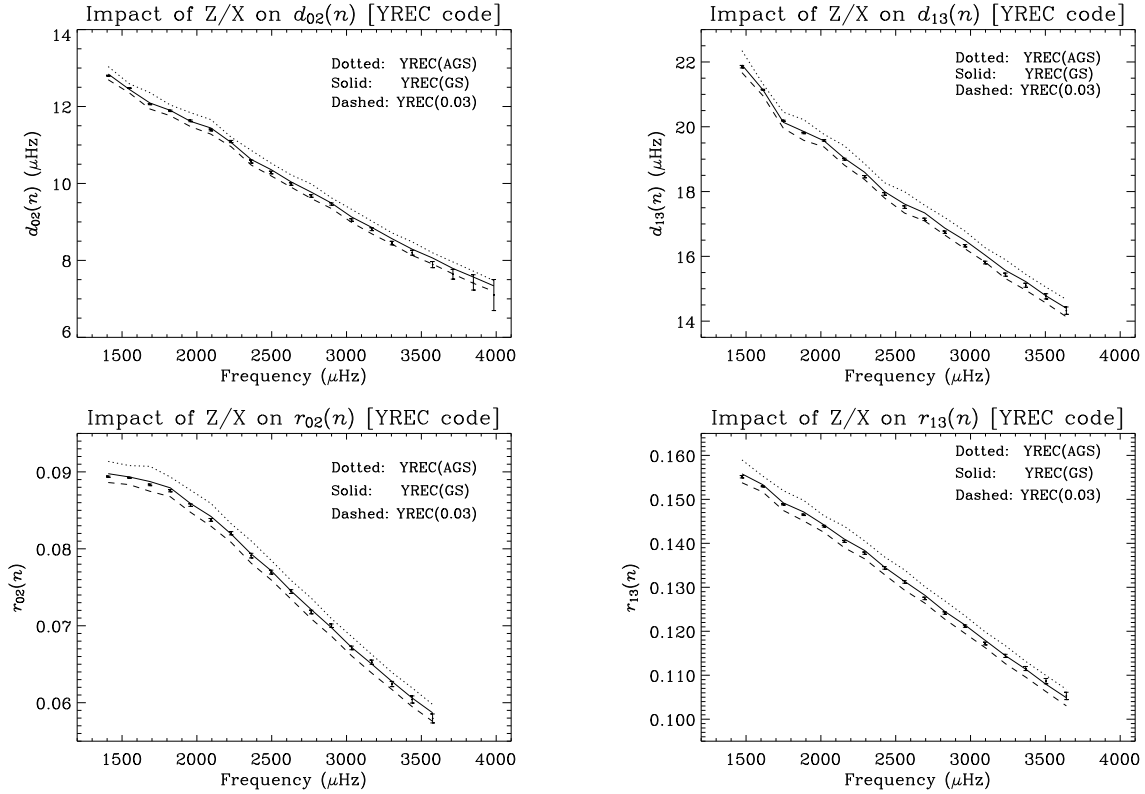


Fig. 8.— Impact of changes to Z/X in the models. The upper panels show the fine spacings of three models computed with the YREC evolution code and the OPAL equation of state, but with different Z/X . Solid line: model YREC(GS), with $Z/X = 0.0229$. Dotted line: model YREC(AGS), with $Z/X = 0.0165$. Dashed line: model YREC(0.03), with $Z/X = 0.03$. Lower panels: same, but for the separation ratios.

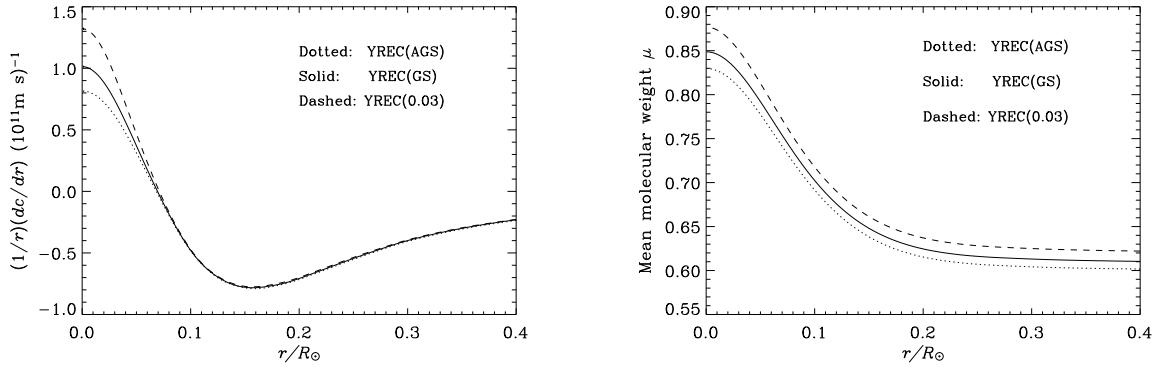


Fig. 9.— Left-hand panel: The function $(1/r)(dc/dr)$ for the three YREC models. This function determines to a large extent the fine spacings, and therefore also the separation ratios. Right-hand panel: The mean-molecular weight profile of the three YREC models.